Oxygen Effects on the EPR Signals from Wood Charcoals: Experimental Results and the Development of a Model

Oleg Y. Grinberg,[†] Benjamin B. Williams,[†] Andres E. Ruuge,[‡] Stalina A. Grinberg,[†,||] Dean E. Wilcox,[‡] Harold M. Swartz,[†] and Jack H. Freed*[,§]

EPR Center for the Study of Viable Systems, Dartmouth Medical School, Hanover, New Hampshire 03755, Department of Chemistry, 6128 Burke Laboratory, Dartmouth College, Hanover, New Hampshire 03755, and National Biomedical Center for Advanced ESR Technology, Department of Chemistry and Chemical Biology, B-52 Baker Laboratory, Cornell University, Ithaca, New York 14853

Received: April 4, 2007; In Final Form: August 31, 2007

Charcoals prepared from certain tropical woods contain stable paramagnetic centers, and these have been characterized by EPR spectroscopy in the absence and presence of oxygen. The EPR-detectable spin density has been determined, as has been the temperature- and frequency-dependence of the oxygen broadening of the EPR signal, which is orders of magnitude larger than that observed with other materials, such as lithium phthalocyanine. Three Lorentzian components are required to fit the char EPR spectrum in the presence of oxygen, and the oxygen-dependence of the line width, intensity, and resonance position of the three components have been quantified. These results and the properties of porous carbonaceous materials are used to develop a model to explain the effect of oxygen on the char EPR spectral properties. The model is based on oxygen adsorption on the char surface according to a Langmuir isotherm and a dipolar interaction between the paramagnetic adsorbed gas and the charcoal spins. The three EPR components are correlated with the three known classes (sizes) of pores in charcoal, with the largest line broadening attributed to dipolar relaxation of spins in micropores, which have a larger specific surface area and a higher concentration of adsorbed oxygen. An attenuated, but similar, EPR response to oxygen by chars when they are immersed in aqueous solution is attributed to water competition with oxygen for adsorption on the char surface.

Introduction

The quantitative measurement of oxygen levels in living tissue has important clinical and research applications, and EPR oximetry has considerable potential for these measurements. This technique requires a material with EPR-detectable paramagnetic centers[1] and involves a concentration-dependent perturbation of the EPR spectral properties by oxygen ($^3\Sigma_g$ groundstate). A number of molecular radicals (e.g., nitroxyl and triarylmethyl) and materials with paramagnetic centers, including certain carbon blacks, coals, charcoals, and crystals of lithium phthalocyanine (LiPc), have been studied for their potential as probes for EPR oximetry. The EPR spectra of nitroxyl or triarylmethyl radicals in aqueous solution typically exhibit ∼0.5 mG/μM broadening by dissolved oxygen. However, certain charcoals prepared from tropical hardwoods by means of controlled pyrolysis[2] contain EPR-detectable species that can exhibit 50−100 mG/μM broadening by dissolved oxygen, and this response is even larger in the gas phase.

Successful implementation of in vivo EPR oximetry requires the development of oxygen-sensitive paramagnetic materials with optimized properties. Currently, LiPc and related compounds are widely used, but there are several criteria (sensitivity, stability, reversibility, selectivity, etc.) that need to be optimized for specific applications of EPR oximetry. In particular, there is a need for materials with increased sensitivity to oxygen at low levels found in tumors and at higher levels found in the brain. To rationally develop these materials requires an understanding of the physical basis and mechanism of oxygen effects on the char paramagnetic centers. Further, this understanding may help to improve the analysis of in vivo data by incorporating physical principles into the spectral model.

Charcoals have certain physical properties that are relevant to their interaction with gases. They are highly porous materials, as seen in scanning electron micrographs of samples prepared from tropical hardwoods (Figure 5 in ref 2), with a specific surface area that is inversely proportional to the pore diameter. Charcoal pores are generally classified by their diameter into three sizes, macropores (>50 nm), mesopores (50−2 nm), and micropores (<2 nm).[3] In addition, they are hydrophobic materials with poor water penetration, particularly into smaller pores. Finally, chars are known for their ability to adsorb gases on their large surface area.

In this study, several measurements have been made of the effect of oxygen on the EPR spectral properties of wood charcoals. These include quantifying the concentration of spins and determining the temperature- and frequency-dependence of the EPR spectrum. Three components are required to fit the O_2-broadened EPR spectrum of the chars, and the oxygen dependence of the line width, intensity, and resonance position of the three components have been measured.

A model, which is based on the properties of charcoals and EPR relaxation mechanisms and which starts with a Langmuir isotherm for O_2 adsorption, has been developed and evaluated with these data. The experimental results are consistent with a

---

* To whom correspondence should be addressed.

[†] Dartmouth Medical School.

[‡] Dartmouth College.

[§] Cornell University.

[||] Deceased.

10.1021/jp072656l CCC: $37.00

dipolar interaction between adsorbed O_2 and the char spins, and the three EPR spectral components correlate with the three classes (sizes) of pores that have different specific surface areas. EPR line broadening in these materials, therefore, appears to correlate with char surface area and the concentration of adsorbed oxygen.

Experimental Section

Wood Charcoals. Charcoals made of metopium (M) and violacea (V) tropical woods were synthesized according to a previously described methodology.[4] The properties of the charcoal depend on the starting material but are also strongly affected by the temperature and time of heating and by the gas atmosphere in the furnace. Samples were heated in a flowing gas mixture of 20% NH_3 in N_2 or 20% CH_4 in N_2 with the temperature increasing at a rate of 10 °C per hour to a maximum of 595 °C, which was maintained for 2 h. After cooling, sizing, and washing (agitation in water) to remove ultrafine material, the chars were reheated at 620 °C for 2 h in the 20% CH_4 in N_2 gas mixture. Samples are indicated by the heating and reheating gas (e.g., V(a/m) is violacea heated in ammonia and reheated in methane).

Density of the chars was estimated by measuring the volume of samples of known mass. Samples were immersed in a small amount of water in a glass capillary with i.d. $= 1.83 \pm 0.05$ mm, and the mass of the char and water was determined. The char was then dried in an oven at 100 °C, cooled, and weighed. Finally, the volume of the char was determined from the mass and volume of the water. The density of the chars was consistently found to be approximately, but slightly greater than, that of water, 1 g/cm^3. This value is somewhat smaller than the 2.2 g/cm^3 reported for peltogyne charcoal[5] and may reflect an overestimation of the char volume by the inability of water to penetrate the smaller pores.

An estimate of the average thickness of the walls of the pores was made by dividing the specific volume of the char, $\sim$1 cm^3/g, by its surface area, 6×10^2 m^2/g.[6] This leads to an average value of 20−30 Å for the wall thickness. However, nonuniform thickness, with thinner walls in the more porous regions, is expected.

EPR Measurements. EPR measurements were obtained on a Varian X-band EPR spectrometer equipped with a temperature controller and a home-built L-band EPR spectrometer.[7] Stability of the spectrometers was verified with a stable reference sample. Measurements were made on $\sim$0.5 mg samples of charcoal placed in oxygen-permeable i.d. = 0.8 mm Teflon tubing (Zeus, Raritan, NJ). The oxygen was varied with a continuous gas flow using different commercially supplied mixtures (Airgas, Bellmawr, NJ) consisting of 0, 0.5, 1, 2, 5, 10, 15, 21, and 26% oxygen in nitrogen ($\pm$0.02% precision). Measurements of the charcoal in water involved filling the Teflon tube containing the sample with water, whereupon it took about 1 h to reach equilibrium. In addition to oxygen concentrations used in the gas phase measurements, samples immersed in water were also measured in 100% oxygen. Spectra were typically collected at 25, 37, and 58 °C and were acquired with low incident microwave power to avoid saturation broadening and a modulation frequency of 100 kHz (24 kHz at L-band). For each spectrum, the modulation amplitude was set to <10% of the observed peak-to-peak line width (LW_{pp}) and the scan range was set to 10−20 times LW_{pp}, depending on the signal-to-noise ratio. From 3−10 separate EPR spectra were collected for each set of conditions, and the mean and standard error of the measured parameters were estimated. A reference sample consisting of a freshly prepared aqueous solution of TEMPONE, 4-oxo-2,2,6,6,-tetramethylpiperidine-d_{18}-1-^{15}N-oxyl (Cambridge Isotopes, Andover, MA), was used to determine the EPR-detectable spin density of charcoal samples.

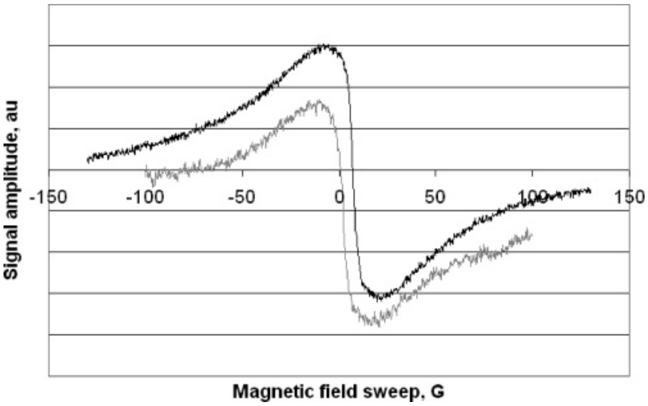

Figure 1. Ambient temperature X-band (black, wider sweep) and L-band (gray) EPR spectra of violacea (V(m/m)) charcoal in a 10% O_2 atmosphere.

EPR spectra were analyzed with EWVoigt software (Scientific Software Services, Bloomington, IL). The spectra were fitted with two or three centers (components), where the position, intensity (double integral), and line width from each component, as well as the relative percentage of absorption and dispersion of the signal, were adjustable fitting parameters. Analysis was performed separately on each set of data, and the average of three characteristic values, the line width, intensity, and resonance position (g value), are reported for each component.

Results

The X-band EPR spectrum of charcoal samples at ambient temperature in the absence of oxygen is a Lorentzian signal only a few tenths of a gauss wide, with LW_{pp} that depends to some extent on the wood and synthesis conditions. Although the identity of the paramagnetic moiety or moieties is not known, the spectral properties are consistent with an $S = {}^1/_2$ spin system. The concentration of EPR-detectable centers in the charcoals was determined both in a nitrogen gas atmosphere and immersed in anaerobic water, and found to be $2 - 5 \times 10^{17}$ cm^{-3} (3−8 $\times 10^{-4}$ M).

At low oxygen levels (<1%), a fit of the char EPR spectrum requires two Lorentzian components (two centers fitting) with different line widths and intensities but a similar g value. Both components are broadened by oxygen, but the wider component is always broadened to a larger extent, which is consistent with previous observations.[8]

Figure 1 shows the superimposed X-band and L-band EPR spectra of violacea charcoal in a 10% oxygen atmosphere at room temperature. These spectra demonstrate that the resonance frequency does not affect the line shape.

EPR measurements at higher oxygen levels require three Lorentzian components to accurately fit the data, and a detailed study was conducted exclusively at X-band because of instrumentally limited sweep width and lower signal-to-noise with the L-band spectrometer. Figure 2 shows a representative 10 °C EPR spectrum of V(m/m) in 26% oxygen, its fit with three Lorentzian lines (three centers fitting), and the low residual indicating the goodness of the fit. Therefore, all spectra of charcoal samples in gas phase with ≥0.5% O_2 were fitted using three centers, which are designated the narrow, medium, and wide components. Charcoal samples immersed in water exhibit similar EPR spectra that also require three Lorentzian compo-

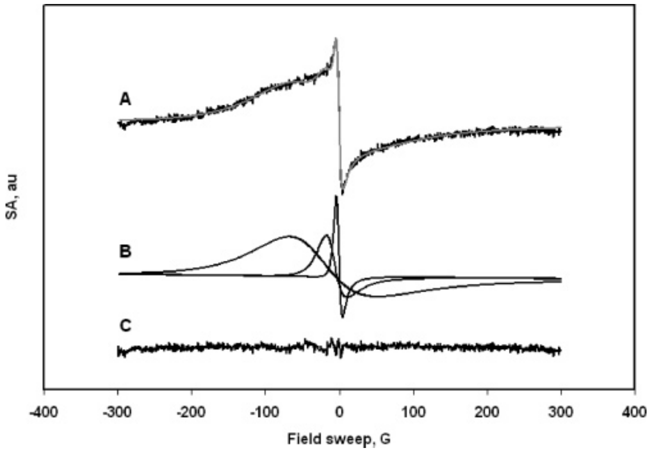

Figure 2. Three component fitting of the 10 °C X-band EPR spectrum of V(m/m) charcoal in a 26% O_2 atmosphere; (A) experimental spectrum, (B) three best fit components, and (C) residual after subtraction of the three best fit components from the experimental spectrum.

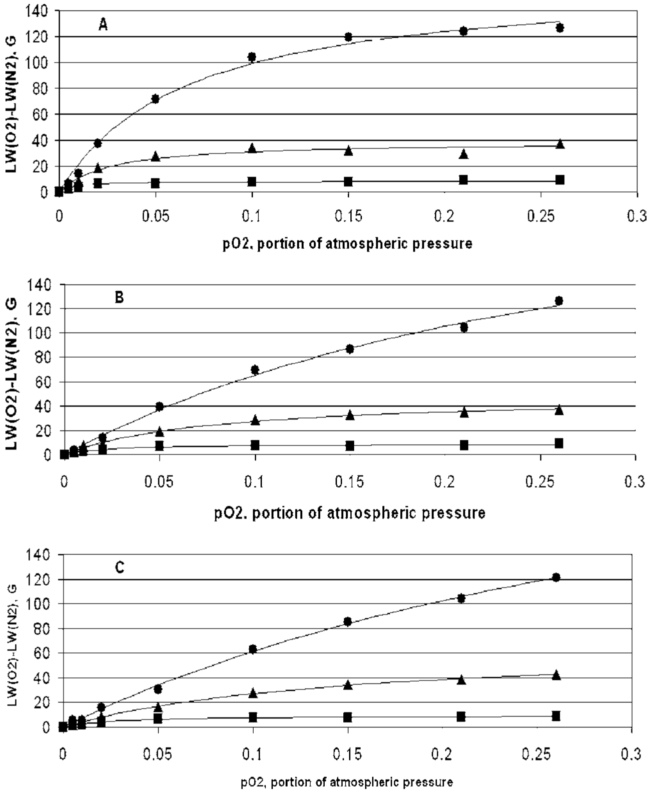

Figure 3. Effect of oxygen on EPR line broadening, $\Delta LW = LW_{pp}(O_2) - LW_{pp}(N_2)$, of the narrow (squares), medium (triangles), and wide (circles) components from fitting of the EPR spectra of V(m/m) charcoal at (A) 25.2, (B) 37.0, and (C) 57.8 °C. Solid lines are the results from fitting with eq 9.

nents, but the line widths are somewhat narrower than those in air for the same oxygen level.

Figure 3 shows the effect of oxygen on the EPR line width of V(m/m) samples at three temperatures (25.2, 37.0, and 57.8 °C), presented as line broadening ($\Delta LW = LW_{pp}(O_2) - LW_{pp}(N_2)$) of the narrow, medium, and wide components derived from three centers fitting of the EPR spectra. As a reference point, the line width of the wide component is found to be ~100 G in air (21% O_2) at 37 °C. In all cases, it is observed that the line widths of all three components initially increase with increasing pO_2 and then level off, suggesting saturation in the order narrow < medium < wide. It is also important to note that the line widths in the lower pO_2 (unsaturated) regime decrease with increasing temperature, whereas the asymptotic limits approached at higher pO_2 (saturation values) appear to be nearly temperature independent.

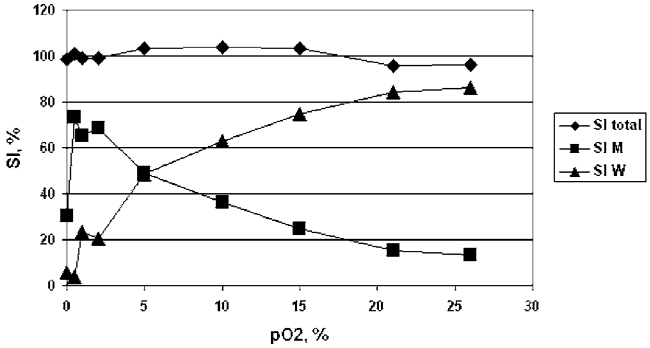

Figure 4. Effect of oxygen on the 57.0 °C total EPR signal intensity (SI total) of V(m/m) charcoal, relative to the intensity at 0% pO_2, and the relative signal intensity percentages of the medium (SI M) and wide (SI W) components.

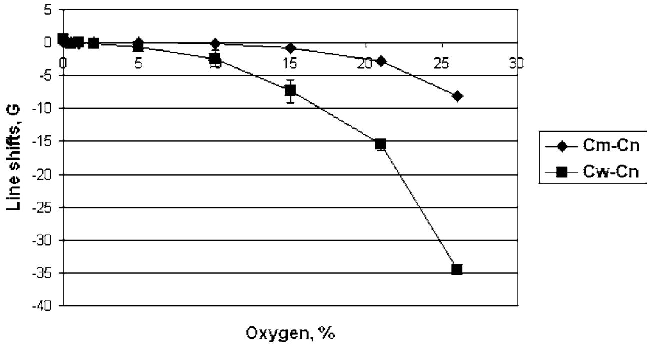

Figure 5. Effect of oxygen on the resonance position at X-band, indicated by a shift of the center field (*C*, in Gauss) of the medium (m) and wide (w) components relative to the narrow (n) component, $C_m - C_n$ and $C_w - C_n$, respectively, for V(m/m) charcoal at 37.0 °C.

The intensity of the EPR signal is proportional to the number of EPR-detectable spins in the charcoal sample and should not depend on the oxygen level. Although this is true for the total signal intensity (Figure 4), there is a significant decrease in the intensities of the narrow and medium components and a corresponding increase in the intensity of the wide component with increasing oxygen. As shown in Figure 4, the wide component becomes about 85% of the total signal at 26% oxygen, whereas the medium component decreases to about 14%. Despite the fact that the narrow component is less than 1% of the total signal at ≥21% O_2, it has the largest amplitude and defines the peak-to-peak line width of the spectrum, as seen in Figure 2. Similar results are found when the charcoals are placed in water, but higher O_2 levels are required to achieve the same intensity percentages.

Spectral deconvolution and fitting of the individual components allows the effect of oxygen on the EPR resonance position to be determined for each component. Although there is some uncertainty in the absolute *g* values of the individual components, the relative *g* values can be determined with some confidence. As shown in Figure 5, an increase in oxygen results in significant shifts to larger *g* values by the medium and wide components, relative to the narrow component. Shifts in the resonance positions of the spectral components when the char is immersed in aqueous solution are insignificant at <26% O_2, although sizable shifts for V(m/m) are found in water at 100% O_2 ($C_{medium} - C_{narrow} = -4.40$ G; $C_{wide} - C_{narrow} = -28.0$ G).

TABLE 1: Ratio of the Initial Slope of the Line Width in the Gas Phase to the Initial Slope of the Line Width in Water for Different Charcoals at 37 °C

chars	M(a/m)	M(m/m)	V(a/m)	V(m/m)
ratio	9.8	7.4	11.3	5.7

Charcoals exhibit a lower sensitivity to oxygen when they are immersed in water than when they are surrounded by oxygen in the gas phase, and the initial slope of the line broadening ($\Delta LW_{pp}/\%O_2$) can be used to quantify this decrease in sensitivity. Table 1 shows the ratio of this value in the gas phase to that in water for different charcoals. Surprisingly, these data suggest that, despite the fact that all samples were reheated in the same methane atmosphere, materials originally made in an ammonia atmosphere have a lower sensitivity to oxygen in an aqueous environment.

Discussion

In this study, several different types of EPR spectral data, and other physical measurements, have been made on charcoals prepared from violacea and metopium tropical hardwoods to evaluate the mechanism for their spectral response to oxygen. Although most of these measurements involved varying the oxygen in the gas phase, some have involved varying oxygen in the gas surrounding a water solution containing the char. This situation, which more closely mimics the biological condition, gives results that are similar to those found in the gas phase, although shifted to somewhat higher O_2 levels. Since these charcoals have some of the largest observed increases in EPR line width upon exposure to oxygen, they may be uniquely suited as probes for in vivo EPR oximetry. However, to optimize this potential, it is important to understand the physical nature of the interaction of oxygen with the paramagnetic centers in these materials.

Another study has measured the effect of oxygen on the EPR spectral properties of charcoals prepared from peltogyne tropical hardwood and developed a model for this interaction.[5] A spin density of 5×10^{19} g^{-1} was measured for the peltogyne samples, which should result in a significant intrinsic dipolar interaction between the spins and a predicted dipolar-broadened EPR line width of ~10 G. Since the experimental line width in the absence of oxygen was only a few tenths of a gauss, the model started with an intrinsic exchange interaction between the char spins that led to the observed narrow EPR signal. The spin density of the violacea and metopium charcoals used in this study, however, is 2 orders of magnitude smaller, and the spin concentration is low enough that dipolar interaction between the char spins is negligible. Therefore, there is no need to invoke an intrinsic exchange interaction between the charcoal spins in these samples.

Building on the physical properties of charcoals, particularly their highly porous structure and their known adsorption of gases, a model for the effect of oxygen on their EPR signals is proposed. Since electronic relaxation, and thus the EPR spectral properties, of a paramagnetic species can be perturbed by another paramagnet through dipole−dipole interaction and/or Heisenberg exchange interaction, it is important to determine the origin of this spin−spin interaction. The temperature dependence of the oxygen-induced EPR line broadening (Figure 3), as well as its magnitude, establishes that this is predominantly a dipolar interaction between the charcoal spins and the paramagnetic O_2 molecules (Appendices A and B). With this fundamental property established, a model is developed for the interaction of oxygen with the charcoal spins, followed by a critical evaluation of its ability to explain the experimental data.

Development of the Model. *Adsorption/Desorption of Gases on the Charcoal Surface.* Wood charcoals are well-known to be extremely porous materials. By a widely accepted classification, pores in activated carbonaceous materials are categorized by size into macropores (>50 nm), mesopores (2−50 nm), and micropores (<2 nm).[3] The porosity of chars, however, depends on the parameters of their synthesis, especially the temperature of carbonization.[9] Of relevance to this study, the charring temperature, along with other factors (heating profile and duration, gas atmosphere), also significantly affects the concentration of paramagnetic species in the char and their sensitivity to oxygen.[10] Because of their porous nature, charcoals have a high surface area that, depending on the material, has been found to be as large as 800 m^2/g.[3]

A well-known feature of charcoals is their physical adsorption of gases. In the simplest case, adsorption/desorption processes can be described by the Langmuir isotherm. Following Adamson,[11] the equilibrium concentration of oxygen adsorbed on a charcoal surface is

$$[O_2]^{ads}\frac{1}{\tau} = \frac{\sigma N_a P}{\sqrt{2\pi MRT}}\left(\frac{S}{\sigma} - [O_2]^{ads}\right) \tag{1}$$

where, in SI units, $[O_2]^{ads}$ is the concentration of adsorbed oxygen (molecules/kg), τ is the average surface residence time of an oxygen molecule, σ is the area occupied on the surface by one adsorbed oxygen molecule, N_a is Avogadro's number, P is the partial pressure of oxygen in the gas phase, $M = 0.032$ kg/mol is the molar mass of the oxygen molecule, R is the universal gas constant, T is the absolute temperature, and S is the specific surface area of the char (m^2/kg). Rearranging eq 1 gives the concentration of adsorbed oxygen as a Langmuir isotherm

$$[O_2]^{ads} = B\frac{bP}{1 + bP} \tag{2}$$

where $B = S/\sigma$ and $b = \tau\sigma N_a/(2\pi MRT)^{1/2}$. Although the Langmuir relationship has several simplifying assumptions and real adsorption/desorption processes are often more complex, this is a reasonable starting point.

Further development of this model involves the assumptions that $\tau = \tau_0 \exp(Q/RT)$, where Q is the energy of gas desorption, $\tau_0 \approx 10^{-13}$ s is the vibration period of the O_2 molecule, and σ for an oxygen molecule is similar to the value for a nitrogen molecule, 16.2×10^{-20} m^2. Charcoals are known to have a relatively small energy of interaction with adsorbed molecules. Vartapetyan et al.[6,12] studied charcoals synthesized from tropical hardwoods, similar to those in this study, and reported surface areas of $S = 550-650$ m^2/g and desorption energies of $Q = 29.6-30.4$ kJ/mol for nitrogen molecules at 77 K. This allows an estimation of $\tau \approx 20$ ns for oxygen molecules at 310 K. Using these values for σ and τ, $S = 6.0 \times 10^5$ m^2/kg, and eq 2, it is possible to predict that charcoal in equilibrium with air (21% O_2) at 310 K and standard atmospheric pressure has a surface concentration of adsorbed oxygen of $[O_2]^{ads} \approx 2.4 \times 10^{24}$ molecules/kg. The associated Langmuir parameters are $B = 3.7 \times 10^{24}$ kg^{-1} and $b = 8.6 \times 10^{-5}$ Pa^{-1}.

EPR Line Broadening. It is proposed here that the remarkable increase in EPR line width originates from a high oxygen concentration on the charcoal surface near the paramagnetic centers. This is supported by the fact that the line width broadening approaches an asymptotic limit at high pO_2 (Figure

3), consistent with eq 2 and saturation in the Langmuir isotherm description. It is assumed that the charcoal spins do not interact, which is reasonable if they are homogeneously distributed at low concentration, and this appears to be a valid assumption for these samples, based on the spin density measurements.

As indicated by the decrease in EPR line broadening by oxygen as the temperature increases in the low pO_2 regime (Figure 3, and Appendices A and B), there is predominantly a dipolar interaction between the charcoal spins ($S = {}^1/_2$) and adsorbed oxygen ($S = 1$). To further develop this model, two limits for the EPR line broadening by oxygen need to be considered: inhomogeneous broadening and homogeneous broadening.

Inhomogeneous Line Broadening. If the residence time of an oxygen molecule adsorbed on the surface of the char is long and its relaxation time is also long, then dipole−dipole interaction between two unlike spins, I and S, can be described by inhomogeneous broadening, which is given by statistical theory[13]

$$\delta_I = \frac{2\pi^2}{3\sqrt{3}}\gamma_I\gamma_S\hbar N_S \cong 3.8\gamma_I\gamma_S\hbar N_S \tag{3}$$

where γ is the gyromagnetic ratio for the spins, $\hbar$ is Planck's constant, and N_S is the spin density of oxygen molecules. The method of moments gives a similar formula[13]

$$\delta_I = 5.3\gamma_I\gamma_S\hbar N_S \tag{4}$$

The experimentally measured peak-to-peak line width for inhomogeneous line broadening is then predicted to be

$$\Delta LW_{pp} = A[O_2]^{ads} \tag{5}$$

where, in cgs units, $A = 4.9 \times 10^{-20}$ G cm^3 for a random distribution and $A = 5.4 \times 10^{-20}$ G cm^3 for a regular distribution of $S = {}^1/_2$ paramagnetic centers on a lattice. This formula has been verified experimentally in solids and irradiated solids[14,15] and in frozen glass solutions of metal ions in the concentration range from 7.6×10^{18} to 1.1×10^{21} cm^{-3} (0.013−1.8 M).[16] Kobayashi, et al.[17] used the same approach to explain EPR line broadening by O_2 in activated carbon fibers, which are microporous materials having many features common to charcoals. In these cases, molecular oxygen ($S = 1$) requires the correction factor $[S(S + 1)]^{1/2}$ in eq 5.[13]

Homogeneous Line Broadening. If T_1 (and T_2) of O_2 adsorbed on charcoal is short and the adsorbed oxygen diffuses rapidly, then another limit is more appropriate. In such a "motional-narrowing" limit, homogeneous line broadening needs to be considered.[13,18] The complete expression is given by Freed[18] but only the case of very short O_2 relaxation, i.e., $|\omega_0 T_{1,O_2}| < 1$, is considered here

$$T_{2,I}^{\ -1} = \frac{8\pi}{3}\gamma_I^{\ 2}\gamma_S^{\ 2}\hbar^2 S(S + 1)J(0) \tag{6}$$

where the approximation $J(\omega_0) \approx J(0)$ for the spectral density function is valid in this limit. If the diffusion correlation time (Appendix A) is assumed to be similar to the average surface residence time of the oxygen molecules (i.e., $\tau \approx 20$ nsec), then O_2 spin relaxation is dominant, (i.e., $\tau/T_1 \approx 2 \times 10^3 \gg 1$) and $J(0)$ simplifies to the relationship[18] (see Appendix A)

$$J(0) = \frac{2}{3}\frac{N_S}{d^3}T_{1,O_2} \tag{7}$$

Finally, the line broadening in Gauss (cgs units) is

$$\Delta LW_{pp} = \frac{32\pi}{9}\gamma_I^{\ 2}\gamma_S\hbar^2\frac{[O_2]^{ads}}{d^3}T_{1,O_2} = 7.8 \times 10^{-32}\frac{[O_2]^{ads}}{d^3}T_{1,O_2} \tag{8}$$

where $[O_2]^{ads}$ is the concentration (molecules/cm^3) of oxygen adsorbed on the charcoal surface, d is the distance (cm) of closest approach between oxygen molecules and the charcoal spins, and T_{1,O_2} is the oxygen relaxation time (s).

Evaluation of the Model. *Effect of Oxygen on the char EPR Line Width.* Using eq 5 and $[O_2]^{ads} \approx 2.4 \times 10^{21}$ molecules/g of charcoal, which is estimated for standard atmospheric conditions (21% O_2), a line broadening of ~200 G can be estimated. This value compares rather well with the experimental value of $\Delta LW_{pp} \approx 100$ G for the wide component of the char EPR spectrum in air. However, the applicability of eq 5 needs to be considered.

To determine the appropriate physical model requires knowledge of the time scale of the observed phenomenon. In this case, three time scales need to be considered, the residence time of oxygen molecules on the char surface, the inverse of the char-oxygen spin−spin dipolar interaction,[19] and the oxygen relaxation time. The surface residence time of oxygen on chars is estimated to be $\tau \approx 20$ ns, which is appropriate for physisorbed O_2 because the surface diffusion mechanism is expected to involve desorption and readsorption. The oxygen spin−lattice relaxation time, T_{1,O_2}, was measured in water and several other solutions by Teng, et al.[20] using proton spin−lattice relaxation, and found to be approximately 7.5 ps and practically independent of solvent and viscosity. Such a short relaxation time results in a very broad EPR line width for $S = 1$ oxygen and is the reason why an EPR spectrum of oxygen dissolved in fluids has never been reported. Also, T_{1,O_2} is much shorter than the period of the Larmor precession, which is 0.1 and 0.8 ns for X- and L-band EPR, respectively, further justifying the assumption $J(\omega_0) \approx J(0)$ in eq 6.

Equations 3−5 represent the static limit and inhomogeneous broadening and are appropriate only if the spin relaxant, O_2, has a relatively long T_1, compared to its dipolar interaction with the char spins, and O_2 diffusion on the char is very slow. The T_1 for adsorbed O_2 is expected to be comparable, at least in order of magnitude, to values measured in solution by Teng, et al.,[20] and thus, eq 8 is more appropriate than eq 5. As a first approximation, it is assumed that T_1 for O_2 adsorbed on the char is 7.5 ps and that T_1 and d are (nearly) constant within the range of experimental temperatures. Using accepted values for the various parameters, the estimated equilibrium concentration of oxygen on the char surface ($[O_2]^{ads} \approx 2.4 \times 10^{21}$ molecules/g), the char density (~1 g/cm^3) and eq 8, it can be estimated that $d \approx 2.5$ Å for the observed ~100 G broadening of the wide component. This value of d, which is in the range of van der Waals contact, suggests that char spins are located primarily on or near the surface, resulting in close contact with adsorbed O_2. However, a somewhat larger value of d would be obtained if T_1 for adsorbed O_2 is longer than it is for freely diffusing O_2 in solution or if the value of $[O_2]^{ads}$ is larger than estimated. The latter is likely to be the case because of the low value that was determined for the average char density and it may be especially true for micropores that are associated with the wide spectral component (see below).

TABLE 2: Best Fit Values of the eq 9 Parameters C_x and b_x, where x Indicates the Narrow (n), Medium (m), and Wide (w) Components of the EPR Spectra of V(m/m) Samples, at Different Temperatures

parameter	25.2 °C	37.0 °C	57.8 °C
$C_n \times 10^2$, G/Pa	1.26	0.43	0.37
$C_m \times 10^2$, G/Pa	1.51	0.64	0.45
$C_w \times 10^2$, G/Pa	2.47	0.85	0.76
$b_n \times 10^5$, Pa^{-1}	149.0	48.8	39.7
$b_m \times 10^5$, Pa^{-1}	38.8	13.2	6.7
$b_w \times 10^5$, Pa^{-1}	15.0	3.1	2.4
C_n/b_n, G	8.5	8.9	9.4
C_m/b_m, G	38.9	48.5	67.2
C_w/b_w, G	165.2	276.4	311.1

TABLE 3: Energy of Oxygen Desorption, Q, (mean ± SD) and the Ratio of the Average Value of C/b for the Medium and Wide EPR Components to the Average C/b Value for the Narrow Component of V(m/m)

component	Q, kJ/mol	$(C_x/b_x)/(C_n/b_n)$ ($\propto S_x/S_n$)
narrow	29.7 ± 17.3	1.0
medium	41.4 ± 11.4	5.7 ± 1.3
wide	41.0 ± 25.0	27.9 ± 7.4

The combination of eqs 2 and 8 gives the following relationship for line broadening with this model:

$$\Delta \mathrm{LW}_{\mathrm{pp}} = C\frac{P}{1 + bP} \qquad (9)$$

where $C = (7.82 \times 10^{-32}\ T_{1,\mathrm{O}_2}/d^3)(S/\sigma)b$ and b is defined in connection with eq 2. The numerical values of these parameters at 37 °C (310 K), using SI units of Pa for pressure, are $C = 0.948 \times 10^{-2}$ G/Pa and $b = 8.6 \times 10^{-5}$ Pa^{-1}.

The solid lines in Figure 3 show the result of fitting the experimental data with eq 9, and the best fit parameters for the three components at the three temperatures are given in Table 2. Considering the simplifications, assumptions and approximations of the model, there is reasonably good agreement between the predicted and the experimental values of C and b, particularly those of the wide component.

Results of this fitting show the significant effect of temperature on the model parameters, as expected. The decrease in the values of C and b with increasing temperature is consistent with the decrease in τ as the temperature increases. The temperature dependence of b allows an estimation of the energy of O_2 desorption, Q, which is given in Table 3 for the three components. The C/b ratio is proportional to surface area, S, and T_{1,O_2} according to eq 9. If, as considered below, it is assumed that T_{1,O_2} is similar for the different components, then the ratio of the pore surface areas, S_m/S_n and S_w/S_n, can be estimated from the ratio of the average values of C/b for each component. Table 3 includes these surface area ratios, as estimated from the parameters obtained from fits of the EPR data and this model.

Based on 77 K N_2 adsorption isotherms, it has been reported that charcoals made from peltogyne wood under a range of similar conditions (600−660 °C heating under different gases) have total surface areas and mesopore surface areas of 550−680 and 6−20 m^2/g, respectively, and a gas desorption energy of $Q = 26{-}38$ kJ/mol.[6] The Table 3 values of Q for O_2, which are derived from 25 to 58 °C EPR data, are in good agreement with N_2 values for similar charcoals, and estimates of the pore surface area ratios that are derived from this model are also reasonably consistent with reported surface areas, considering the uncertainty and approximations. Thus, estimates from this analysis further support the correlation of narrow, medium, and wide EPR components with the paramagnetic centers located in macropores, mesopores and micropores, respectively.

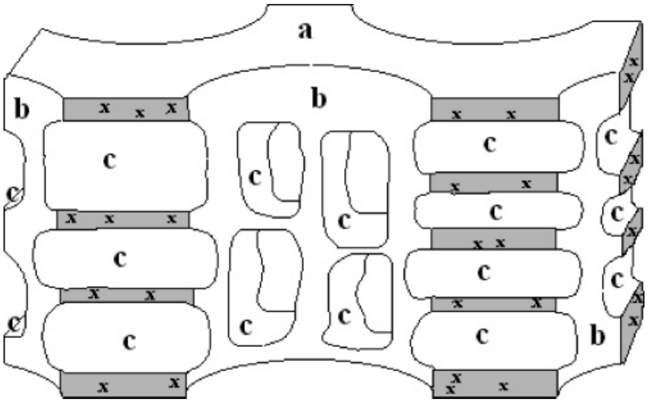

Figure 6. Representation of char cross sections from regions with macropores (a), mesopores (b), and micropores (c), with EPR-detectable char species indicated by X's.

Effect of Oxygen on the Char EPR Signal Intensity. To explain the observed variation in signal intensity of the three components with increasing pO_2, it is assumed that the charcoal spins are randomly distributed on, or just below, the surface of the pore walls and that the number of charcoal spins located in the different pores is proportional to the pore surface area, micropores > mesopores > macropores, as indicated in Figure 6. Further, the Langmuir binding isotherm requires that the concentration of adsorbed oxygen depends on the surface area, as well as the oxygen partial pressure.

Two limits of pO_2 are considered. At low oxygen levels, all char spins have a dipolar interaction with a similar low concentration of surface adsorbed oxygen. In this limit, the EPR spectrum should be insensitive to the pore structure and all charcoal spins would contribute to the narrow component. At higher oxygen levels, there will be a larger amount of adsorbed oxygen in regions of the char with higher specific surface area, resulting in a greater dipolar interaction with the spins located in the micropores. According to eq 2, pores with a smaller surface area will have a lower concentration of adsorbed oxygen than pores with a larger surface area. It is observed (Figure 3) that the line width of the narrow EPR component reaches a plateau at ∼5% O_2, suggesting that this is the pO_2 at which spins in the macropores achieve a maximum dipolar interaction with surface adsorbed oxygen. As pO_2 increases, the amount of oxygen that is adsorbed in the char that contains pores with a larger surface area increases, as does the dipolar interaction with spins in these volumes of the char. The data in Figure 4 suggest that about 1%, 14%, and ∼ 85% of the spins are located in the charcoal containing macropores, mesopores, and micropores, respectively.

A number of factors can affect the interaction between charcoal spins and oxygen molecules. Teng and Bryant[21] measured the paramagnetic contributions of freely diffusing oxygen to the proton spin−lattice relaxation of the enzyme ribonuclease A in solution. They found several regions of the protein where oxygen enhancement of the relaxation rate is quite large. Recently Teng et al.[22] have suggested that perturbation of the proton spin−lattice relaxation by freely diffusing oxygen provides a direct measure of solvent accessibility to the protein surface. Since the electron relaxation time is much shorter than electron−nuclear coupling correlation times, the proton spin relaxation rates appear to correlate with the local oxygen concentration. Extending this to charcoals, broadening of the char EPR line width by adsorbed oxygen may be analogous to the paramagnetic O_2 contributions to nuclear spin−lattice relaxation in proteins. Thus, the different pore sizes in wood charcoals appear to correlate with different oxygen accessibility to the charcoal spins and can explain the effect of oxygen on the relative signal intensity and line width of the components of the EPR signal.

Effect of Oxygen on the g Value of the Char EPR Signal. There are two plausible explanations for the shift in resonance conditions with increasing oxygen. A reversible oxygen-induced change in the structure of the charcoal paramagnetic centers could alter the *g* value. More likely, however, this is a dynamic frequency shift (DFS),[13] for which homogeneity of line broadening is an important parameter. If spin relaxation is dominated by the T_1 of O_2, then EPR measurements at different frequencies could evaluate whether the change in resonance position as a function of O_2 is due to a DFS. Unfortunately, the short field sweep of our L-band spectrometer does not allow accurate measurement of field shifts at higher oxygen concentrations, but high field EPR measurements may provide data to evaluate whether there is a DFS.

Temperature Dependence of the Char EPR Line Broadening. The results for Q in Table 3, where the residence time of oxygen on the char surface is given by $\tau = \tau_0 \exp(Q/RT)$, are consistent with previously measured desorption rates, as already noted. This provides the correct temperature dependence predicted by this model based on dipolar interactions, whereas Heisenberg exchange interaction (Appendix B) between adsorbed oxygen and the char spins does not. Another potentially temperature-dependent factor in this model is T_{1,O_2}, which has a proportional relationship with C/b. The increase in C/b between 25.2 and 57.8 °C (10%, 73%, and 92% for narrow, medium, and wide pores, respectively) may be due to an increase in T_{1,O_2}, in which case the O_2 relaxation may depend somewhat on the nature of the pore, which is certainly worthy of further study.

Comparison of the Effect of Oxygen in the Gas and Aqueous Phases. The decrease in oxygen sensitivity of the chars when they are immersed in water can be explained by a simple model that is valid for dilute solutions and is based on the partitioning of oxygen between a bulk solution and an interface phase[11]

$$O^{w}_{2(O_2\ \text{in water})} + H_2O^{a}_{(\text{adsorbed water})} \rightleftharpoons O^{a}_{2(\text{adsorbed } O_2)} + H_2O^{w}_{(\text{water in solution})} \qquad (10)$$

The equilibrium constant for this process is

$$K = \frac{N^{a}_{O_2} a_{H_2O}}{N^{a}_{H_2O} a_{O_2}} \qquad (11)$$

where a is the activity of H_2O or O_2 in solution, and the activities of the adsorbed species are given by their mole fractions, $N^{a}_{O_2}$ and $N^{a}_{H_2O}$. The concentration of oxygen adsorbed on the charcoal from the water phase is

$$[O^{a}_{2}] = \frac{n_s N_a f[O_2]}{1 + f[O_2]} \qquad (12)$$

where $f = f' \exp(-\Delta H/RT) = K/a_{H_2O}$, n_s is the moles of adsorption sites per kilogram and $\Delta H = \Delta H_{O_2} - \Delta H_{H_2O}$ is the difference between the enthalpies of adsorption of O_2 and H_2O. The ratio of the initial slope in the gas phase to the initial slope in water (Table 1) can be interpreted as the ratio of the activities of O_2 and H_2O in the adsorption layer of the charcoal. In other words, the charcoal spins sense the oxygen concentration adsorbed on the surface, not in bulk solution. The temperature dependence of the initial slope of O_2-induced line broadening in water allows an estimation of the value $\Delta H \approx -7.6$ kJ/mol. Although this is only an approximate value, it indicates additional insight that can be obtained from this model.

Further Tests of the Model. Analysis of the EPR spectra of charcoals includes fitting the signal intensity, line width, and resonance position of two or three components. Since this model correlates oxygen binding by a Langmuir isotherm to dipolar line broadening by the adsorbed oxygen, one test of the model would involve simulation of the EPR line broadening using only $[O_2]^{ads}$ from the Langmuir relationship as a fit parameter. In addition, experiments involving competition with large inert molecules capable of clogging the micropores should preferentially affect the broadest component, since it is attributed to spins located in the micropores where there is the largest surface area density and the most adsorbed oxygen.

Although the analysis with eq 9 has several assumptions and simplifications, a key feature of the model is the short oxygen T_1, which results in a bona fide relaxation mechanism leading to homogeneous broadening of the char EPR spectrum. Therefore, the degree of homogeneity of the broadening is an important issue, which could be addressed with spin−echo measurements. Also a more general theory that bridges the gap between statistical theory (e.g., eq 3) and the motionally narrowed limit (e.g., eq 6), such as that developed by Nevzorov and Freed,[19] might refine this model further. Finally, although the temperature dependence and magnitude of the EPR line broadening is consistent with a dominant dipolar interaction, contributions from Heisenberg spin exchange between O_2 and the char spins should be considered and could be included in a more advanced model, as discussed in Appendix B.

Comparison with Other Models. Other studies have measured the EPR spectral properties of paramagnetic centers in wood charcoals and other carbonaceous materials, and one has proposed a mechanism for line broadening of the EPR signal from peltogyne wood and fructose chars by oxygen.[5] Although some of the reported effects of oxygen on the peltogyne EPR spectrum (e.g., two Lorentzian components at low oxygen, line broadening, and intensity shift to the broader component at higher oxygen levels) are qualitatively similar to those found here, there are significant differences that motivated the development of a different model. In particular, the spin density of the peltogyne char was reported to be 2 orders of magnitude larger than that found here for violecea and metopium chars. This high spin density, along with the narrow line in the absence of oxygen, suggested an intrinsic exchange interaction between the peltogyne char spins, which was perturbed and eventually dominated by a dipolar interaction with the adsorbed oxygen. This model of Atsarkin et al.[5] is not consistent with oxygen effects on the char EPR spectra found in this study, although it may be appropriate for chars with higher spin density and an intrinsic interaction between the paramagnetic centers.

In the model developed here, different spectral components are associated with char spins located in pores of different size, and, therefore, surface area density, and the magnitude of the line broadening is associated with the amount of oxygen adsorbed near the char spin. An alternate model could be based on the interaction of adsorbed oxygen with char spins at different depths from the surface; the broadest component, which has the highest intensity, would be spins located closest to the surface and narrower components would be spins located further from the surface, which would have a weaker dipolar interaction with adsorbed oxygen. Whether there is evidence for three distinct depth components or experimental data that could distinguish this alternate model from the current model is unclear.

Summary

The EPR spectral properties of paramagnetic centers in charcoals from tropical hardwoods have been characterized in the presence of different levels of oxygen. While a single Lorentzian will adequately fit the signal in the absence of oxygen, two and ultimately three Lorentzian components are required to fit the spectrum with increasing oxygen. These three components have different line widths, intensities, and resonance frequencies that vary with oxygen. The overall O_2-broadened EPR spectrum has the same line shape at different microwave frequencies, and the line broadening decreases with increasing temperature. Finally, the same oxygen effects on the char EPR properties are found when the chars are immersed in water, although higher levels of oxygen are required to elicit the same magnitude of the effects.

A model, based on the highly porous nature of charcoal and its ability to adsorb gases, is developed to explain the experimental results. The Langmuir isotherm is used to quantify O_2 adsorption on the char surface from the gas phase or from oxygen dissolved in water. This results in dipolar interaction between adsorbed O_2 and the char paramagnetic centers, which broadens the char EPR spectrum that is now composed of three spectral components. The three components required to fit the O_2-broadened EPR spectrum are correlated with three classes of charcoal pores, with the narrow, medium, and wide components originating from spins in macropores, mesopores, and micropores, respectively. Oxygen-dependence of the EPR line width and intensity of the three components indicates that the number of char spins and the amount of oxygen that can be adsorbed correlate with the pore surface area density, macropores < mesopores < micropores. Finally, the relative activities of surface-bound water and oxygen attenuate the adsorption of oxygen and lower the oxygen sensitivity of chars when they are dissolved in water.

Acknowledgment. We dedicate this paper to the memory of Stalina A. Grinberg. This work was supported by the NIH/NIBIB Grants "EPR Center for the Study of Viable Systems" P41EB002032 and "Measurement of pO_2 in Tissues *in vivo* and *in vitro*" PO1 EB2180 (to H.M.S.) and NIH/NCRR Grant "National Biomedical Center for Advanced ESR Technology" P41RR016292 (to J.H.F.). We thank Paul Ceroke for synthesis of the char samples.

Appendix A: Dipole−Dipole Interactions

Dipole−dipole interaction between two unlike spins, *I* and *S*, involved in isotropic random motion results in homogeneous broadening in the motional narrowing regime. This describes the interaction of char radicals (*I*) with oxygen molecules (*S*) that diffuse along the char surface with a residence time that is comparable to, or greater than, their spin relaxation time. In this case, line-broadening is given by[13]

$$T_{2,\mathrm{I}}{}^{-1} = \gamma_\mathrm{I}{}^2\gamma_\mathrm{S}{}^2\hbar S(S+1)\left\{\frac{1}{6}J^{(0)}(0) + \frac{1}{24}J^{(0)}(\omega_\mathrm{I} - \omega_\mathrm{S}) + \frac{3}{4}J^{(1)}(\omega_\mathrm{I}) + \frac{3}{2}J^{(1)}(\omega_\mathrm{S}) + \frac{3}{8}J^{(2)}(\omega_\mathrm{I} + \omega_\mathrm{S})\right\} \quad \text{(A1)}$$

where

$$J^{(0)}(0) = \frac{48\pi}{15}J(0) = \frac{16\pi}{5}6J(0) \quad \text{(A2)}$$

$$J^{(1)}(\omega_\mathrm{S}) = \frac{8\pi}{15}J(\omega_\mathrm{S})$$

$$J^{(2)}(\omega_\mathrm{S} + \omega_\mathrm{I}) = \frac{32\pi}{15}J(\omega_\mathrm{S} + \omega_\mathrm{I})$$

The line broadening is then given by

$$T_{2,\mathrm{I}}{}^{-1} = \frac{4\pi}{15}\gamma_\mathrm{I}{}^2\gamma_\mathrm{S}{}^2\hbar^2 S(S+1)\left\{2J(0) + \frac{1}{2}J(\omega_\mathrm{I} - \omega_\mathrm{S}) + \frac{3}{2}J(\omega_\mathrm{I}) + 3J(\omega_\mathrm{S}) + 3J(\omega_\mathrm{I} + \omega_\mathrm{S})\right\} \quad \text{(A3)}$$

The relevant $J(\omega)$ expressions are given by Freed,[18] but here, partly for the sake of simplicity, we consider the case of very short O_2 relaxation, i.e., $|\omega_0 T_{1,\mathrm{O_2}}| < 1$. Equation A3 then simplifies to

$$T_{2,\mathrm{I}}{}^{-1} = \frac{8\pi}{3}\gamma_\mathrm{I}{}^2\gamma_\mathrm{S}{}^2\hbar^2 S(S+1)J(0) \quad \text{(A4)}$$

where the spectral density $J(0)$ ($J(\omega_0) \approx J(0)$ in this limit) is given by

$$J(0) = \frac{8}{27}\frac{N_\mathrm{S}}{dD}\left[\frac{1 + {}^1/_4(\tau/T_1^\mathrm{S})^{1/2}}{1 + (\tau/T_1^\mathrm{S})^{1/2} + {}^4/_9(\tau/T_1{}^S) + {}^1/_9(\tau/T_1^\mathrm{S})^{3/2}}\right] \quad \text{(A5)}$$

where D is the O_2 diffusion coefficient on the char, d is the distance of closest approach of O_2 to a spin on the char, and $\tau = d^2/D$ is a correlation time.

If we assume that O_2 relaxation is dominant (i.e., $\tau/T_1^\mathrm{S} \gg 1$), then $J(0)$ simplifies to

$$J(0) = \frac{2}{3}\frac{N_S}{d^3}T_1^\mathrm{S} \quad \text{(A6)}$$

Appendix B: Spin Exchange

We have emphasized a relaxation mechanism based on dipole−dipole interaction between char radicals and oxygen molecules, but Heisenberg spin exchange (HE) is also an important spin relaxation mechanism.[23,24] HE is a mechanism that requires contact or collisions between a char radical and an oxygen molecule and is a short range interaction, unlike dipolar interactions that have a longer range. Thus, unlike dipolar interactions, it will be ineffective as a source of inhomogeneous broadening in the limit of solids with little or no motion. In the presence of O_2 diffusion (or desorption and readsorption) on the char surface, it becomes a viable broadening mechanism. However, HE typically yields a homogeneous broadening that increases substantially with increasing temperature, whereas the observed broadening decreases with temperature (cf. Table 2 and Figure 6). Such a temperature dependence is characteristic of the well-known behavior of dipole−dipole interactions,[13,18,19,23,24,25] and this is why the latter is emphasized here.

Nevertheless, it is appropriate to briefly comment on the potential relevance of HE to the present study. An expression for the homogeneous line broadening in the case of short $T_{1,\mathrm{O_2}}$ is given in a convenient form by[24]

$$\Delta\mathrm{LW}_\mathrm{HE} = \mathrm{AK}_\mathrm{HE}[\mathrm{O_2}]^\mathrm{ads} \quad \text{(B1)}$$

where

$$K_{\mathrm{HE}} = p_{\mathrm{A}}(4\pi dD) \tag{B1a}$$

and

$$A = 2/\sqrt{3}\gamma_{\mathrm{I}} \tag{B1b}$$

with d and D defined in Appendix A, and p_{A}, which indicates the probability of exchange per collision, given by

$$p_{\mathrm{A}} = \frac{k_{\mathrm{e}}\tau_{\mathrm{c}}}{1 + k_{\mathrm{e}}\tau_{\mathrm{c}}} \tag{B2a}$$

where

$$k_{\mathrm{e}} = \frac{4}{3}J^2 T_{1,\mathrm{O}_2} \tag{B2b}$$

Here J is the exchange interaction between the spins of a colliding O_2 and char spin, and τ_c is the mean interaction time that, in a diffusion model,[23] is given by $\tau_c = \tau/6$, with τ defined in Appendix A. For reasonable values[23,24] of J, τ_c, and T_{1,O_2}, one readily estimates that $p_A \approx 1$ corresponds to "strong HE", for which eq B1 gives

$$\Delta \mathrm{LW}_{\mathrm{HE}} \propto K_{\mathrm{HE}}[\mathrm{O}_2]^{\mathrm{ads}} \propto D[\mathrm{O}_2]^{\mathrm{ads}} \propto \tau^{-1}[\mathrm{O}_2]^{\mathrm{ads}}$$

Let us first consider the limiting case of unsaturated O_2 adsorption, (i.e., $bP \ll 1$ in eq 2). Then $[\mathrm{O}_2]^{\mathrm{ads}} \propto (\tau/T^{1/2})$ so $\Delta\mathrm{LW} \propto T^{-1/2}$ or practically temperature independent over 25−58 °C. Next, we consider the limiting case of saturated O_2 adsorption, (i.e., $bP \gg 1$ in eq 2). Then $[\mathrm{O}_2]^{\mathrm{ads}} \propto T^{-1/2}$, so $\Delta\mathrm{LW} \propto (\tau T^{1/2})^{-1}$ which, predicts an increase in line width with increasing temperature. (Both are contrary to the experimental results which include these limits.)

However, it is reasonable to suppose that HE broadening does make some contribution to the line width of the char spins. Thus, for $\tau \sim 20$ ns, we estimate that $D = d^2/\tau \sim 3 \times 10^{-8}$ cm^2/s, using $d \sim 2.5 \times 10^{-8}$ cm. This gives $\Delta\mathrm{LW}_{\mathrm{HE}} \sim 1.5$ G, compared to the value of ~100 G for dipole−dipole interaction with this value of d (see the main text). Thus, this estimate of $\Delta\mathrm{LW}_{\mathrm{HE}}$ is too small to account for the experimental results.

These estimates, suggesting a much greater role for dipole−dipole interactions, are similar to those from studies on lipid membranes, where dipole−dipole effects dominate at lower temperatures and Heisenberg exchange dominates at higher temperatures.[25] Although this estimate for $\Delta\mathrm{LW}_{\mathrm{HE}}$ indicates a minor contribution, further study is warranted to distinguish between the relative contributions of longer range dipole−dipole and short-range HE interactions.

References and Notes

(1) Swartz, H. M.; Clarkson, R. B. The measurement of oxygen in vivo using EPR techniques. *Phys. Med. Biol.* **1998**, *43*, 1957−1975.

(2) Clarkson, R. B.; Odintsov, B. M.; Belford, R. L.; Ceroke, P. J. Stable particulate paramagnetic materials as oxygen sensors in EPR oximetry. *Biol. Mag. Reson.* **2003**, *18*, 233−257.

(3) Rouquerol, J.; Avnir, D.; Fairbridge, C. W.; Everett, D. H.; Haynes, J. H.; Pernicone, N.; Ramsay, J. D. F.; Sing, K. S. W.; Unger, K. K. Recommendations for the characterization of porous solids. *Pure Appl. Chem.* **1994**, *66*, 1739−1758.

(4) Clarkson, R. B.; Odintsov, B. M.; Ceroke, P. J.; Andenkjar-Larsen, J. H.; Fruianu, M.; Belford, R. L. Electron paramagnetic resonance and dynamic nuclear polarization of char suspensions: surface science and oximetry. *Phys. Med. Biol.* **1998**, *43*, 1907−1920.

(5) Atsarkin, V. A.; Demidov, V. V.; Vasneva, G. A.; Dzheparov, F. S.; Ceroke, P. J.; Odintsov, B. M.; Clarkson, R. B. Mechanism of oxygen response in carbon-based sensors. *J. Mag. Reson.* **2001**, *149*, 1−5.

(6) Vartapetyan, R. Sh.; Voloshcuk, A. M.; Buryak, A. K.; Artamonova, C. D.; Belford, R. L.; Ceroke, P. J.; Kholine, D. V.; Clarkson, R. B.; Odintsov, B. M. Water vapor adsorption on chars and active carbons−oxygen sensors prepared from a tropical tree wood. *Carbon* **2005**, *43*, 2152−2159.

(7) Walczak, T.; Lesniewski, P.; Salikhov, I.; Sucheta, A.; Szybinski, K.; Swartz, H. M. L-band electron paramagnetic resonance spectrometer for use in vivo and in studies of aqueous biological samples. *Rev. Sci. Instrum.* **2005**, *76*, 1−6.

(8) Clarkson, R. B.; Vahidi, N.; Boyer, S.; Wang, W.; Smirnov, A.; Swartz, H. M. Characterization of paramagnetic Probes for In Vivo EPR Oximetry, *Proceedings of the 10th Annual Meeting of the Society of Magnetic Resonance in Medicine*; 1991; p 304.

(9) Ouensanga, A.; Largitte, L.; Arsene, M.-A. The dependence of char yield on the amounts of components in precursors for pyrolysed tropical fruit stones and seeds. *Microporous Mesoporous Mater.* **2003**, *59*, 85−91.

(10) Boyer, S. J.; Clarkson, R. B. Electron paramagnetic resonance studies of an active-carbon - the influence of preparation procedure on the oxygen response of the linewidth. *Colloid Surf. A* **1994**, *82*, 217−224.

(11) Adamson, A. W. *Physical Chemistry of Surfaces*, 5th ed.; Wiley: New York, 1990; pp 777.

(12) Vartapetyan, R. Sh.; Clarkson, R. B.; Odintsov, B. M.; Filippov, A. V.; Skirda, V. D. Porous structure of active carbons determined from the adsorption of water vapors and melting of water and cyclohexane in pores. *Colloid J.* **2000**, *62*, 526−531, Translated from *Koloidniyi Zhurnal (Rus)*, *62*, 590−595.

(13) Abragam, A., *The Principles of Nuclear Magnetism*; Oxford: Clarendon, 1962; pp 599.

(14) Grant, W. J. C.; Strandberg, M. W. Statistical theory of spin-spin interactions in solids. *Phys. Rev. A* **1964**, *135*, A715−A726.

(15) Wyard, S. J. Dipolar broadening of electron spin resonance lines in irradiated solids. *Proc. Phys. Soc. London* **1965**, *86*, 587−593.

(16) Grinberg, O. Y.; Nikitaev, A. T.; Zamaraev, K. I.; Lebedev, Y. S. The concentration effect on the EPR line width of solid solutions VO^{+2} and MoO^{+3}. *J. Struct. Khim. (Rus)* **1969**, *10*, 230−233.

(17) Kobayashi, N.; Enoki, T.; Ishii, C.; Kaneko, K.; Endo, M. Gas adsorption effects on structural and electrical properties of activated carbon fibers. *J. Chem. Phys.* **1998**, *109*, 1983−1990.

(18) Freed, J. H. Dynamic effects of pair correlation-functions on spin relaxation by translational diffusion in liquids. 2. Finite jumps and independent T_1 processes. *J. Chem. Phys.* **1978**, *68*, 4034−4037.

(19) Nevzorov, A. A.; Freed, J. H. Dipolar relaxation in a many-body system of spins of 1/2. *J. Chem. Phys.* **2000**, *112*, 1425−1443.

(20) Teng, C. L.; Hong, H.; Kiihne, S.; Bryant, R. G. Molecular oxygen spin-lattice relaxation in solutions measured by proton magnetic relaxation dispersion. *J. Mag. Reson.* **2001**, *148*, 31−34.

(21) Teng, C. L.; Bryant, R. G. Mapping oxygen accessibility to ribonuclease A using high-resolution NMR relaxation spectroscopy. *Biophys. J.* **2004**, *86*, 1713−1725.

(22) Teng, C. L.; Hinderliter, B.; Bryant, R. G. Oxygen accessibility to ribonuclease A: Quantitative interpretation of nuclear spin relaxation induced by a freely diffusing paramagnet. *J. Phys. Chem. A* **2006**, *110*, 580−588.

(23) Eastman, M. P.; Kooser, R. G.; Das, M. R.; Freed, J. H. ESR Studies of Heisenberg Spin Exchange I: Linewidth and Saturation Effects. *J. Chem. Phys.* **1969**, *51*, 2690−2709.

(24) Molin, Yu. N.; Salikov, K. M.; Zamaraev, K. I. *Spin Exchange*; Springer-Verlag: New York, 1980; pp 242.

(25) Shin, Y.-K.; Ewert, U.; Budil, D. E.; Freed, J. H. Microscopic vs. macroscopic diffusion in model membranes by ESR spectral-spatial imaging. *Biophys. J.* **1991**, *59*, 950−957.